This paper reports a study into estimating the impact of dissolved Si and Cr on the crystalline structure, certain mechanical characteristics, and stability of manganese austenite. The theoretical study was based on the first-principle calculations within a density functional theory (DFT) for austenite structures, which were modeled in the form of 2×2×2 superlattices based on a face-centered cubic lattice.

Atoms in the model superlattices were arranged considering the experimental results from analyzing the Mossbauer spectrum and the X-ray phase analysis of experimental alloys corresponding to high manganese steels. The superlattices that represented the structure of the alloyed austenite contained the C atom in the central octahedral pore, which, relative to the Si(Cr) and Mn atoms, was located in the first and second coordinating spheres, respectively.

The analysis of calculation results reveals that the dissolution of Si and Cr in manganese austenite leads to an increase in the stability of the austenite phase, both according to the results from modeling within the DFT and based on the findings from the thermodynamic analysis. At the same time, the austenite phase is transferred to the region of plastic materials according to the ratio of the volumetric elasticity to shear modules of ≥1.75 (a B/G criterion). Determining the density of electronic states shows that among the structures studied, the lowest number of electrons at the Fermi level, which indicates the highest electrochemical stability, is characterized by manganese austenite alloyed by Cr.

The results of this study provide grounds for expanding the systems of alloying high manganese steels by introducing a significant amount (up to 10 at. %) of Si and Cr, in particular for the application of wear, shock, and corrosion-resistant coatings by the method of electric arc surfacing

Keywords: high manganese steel, first-principle calculations, Mossbauer spectroscopy, alloying elements, wear-resistant coatings

UDC 538.9
DOI: 10.15587/1729-4061.2020.217281

ANALYSIS OF THE EFFECTS OF ALLOYING WITH Si AND Cr ON THE PROPERTIES OF MANGANESE AUSTENITE BASED ON AB INITIO MODELLING

P. Prysyazhnyuk
PhD, Associate Professor*
E-mail: pavlo1752010@gmail.com
L. Shlapak
Doctor of Technical Sciences, Professor*
E-mail: tzn@nung.edu.ua
I. Semyanyk
Postgraduate Student*
E-mail: ztk@nung.edu.ua
V. Kotsyubynsky
Doctor of Physical and Mathematical Sciences, Professor
Department of Material Science
State Higher Educational Institution
"Vasyl Stefanyk Precarpathian National University"
Shevchenka str., 57, Ivano-Frankivsk, Ukraine, 76018
E-mail: kotsuybynsky@gmail.com
L. Troshchuk
Mechanical Engineer
Utility company «Municipal Road Company»
Maksimovicha str., 13, Ivano-Frankivsk, Ukraine, 76006
E-mail: ltroshchuk123@gmail.com
S. Korniy
Doctor of Technical Sciences, Senior Researcher, Head of Department
Corrosion and Corrosion Protection Department
Karpenko Physico-Mechanical Institute
National Academy of Sciences of Ukraine
Naukova str., 5, Lviv, Ukraine, 79060
E-mail: kornii@ipm.lviv.ua
V. Artym
Doctor of Technical Sciences, Professor
Department of Construction and Energy Efficient Buildings**
E-mail: viartym@gmail.com
*Department of Welding**
**Ivano-Frankivsk National Technical University of Oil and Gas
Karpatska str., 15, Ivano-Frankivsk, Ukraine, 76019

Received date 20.09.2020
Accepted date 11.11.2020
Published date 02.12.2020

1. Introduction

High-manganese steels are the most widely used material for the manufacture of parts and the application of coatings for such operational conditions when there are impact-abrasive wear and destruction under the influence of dynamic and cyclical loads. The main structural component of such steels is manganese austenite, capable of intensive deformation

strengthening. Important properties that determine the performance of manganese austenite is its crystalline and electron structure. Its features determine the level of the structure stability, the value of elastic constants, as well as the energy condition of the crystal, and, consequently, the stacking fault energy (SFE) [1]. A value of SFE is a defining characteristic when establishing the fundamental possibility for the deformation strengthening of manganese steels by the twinning-induced plasticity (TWIP) [2] or the transformation induced plasticity (TRIP) [3] techniques. In this case, it is especially important to assess the influence of dissolved alloying elements in manganese austenite on its stability and the physical-mechanical characteristics. In addition, when applying coatings from manganese steels, it is important to assess the effect of alloying on the thermophysical characteristics, which emerge in different procedures for calculating temperature fields [4, 5]. Among these elements, it is important to assess the effects of silicon, which is part of almost all high manganese steels and coatings based on them. Chromium is introduced into such coatings to improve corrosion resistance [6], which is evaluated by electrochemical methods [7, 8].

One common procedure in materials science, which makes it possible to model the crystalline structure and determine its properties in a given time, is the quantum-mechanical calculations within the framework of the density-functional theory (DFT) using a method of nonlocal pseudopotential [9]. Such calculations typically employ software tools such as Vienna Ab initio Simulation Package (VASP) (Austria) [10], Cambridge Serial Total Energy Package (CASTEP) (UK) [11], and others. The main limitations of this procedure are the complexity of modeling unordered solid solutions, which include austenite. This necessitates modeling them in the form of supercells of orderly solid solutions that simulate individual cases of unordered structure. In addition, such calculations are carried out for defect-free structures at 0 K, so only the theoretical values of mechanical characteristics are reflected. In this case, an analysis of real solid solutions produces, basically, a qualitative pattern of the influence of dissolved components.

Studying such materials implies the design of new wear-resistant coatings with composite structures, which is relevant for materials science and tribology.

2. Literature review and problem statement

The construction of new, as well as the continuous improvement of existing algorithms of quantum-mechanical calculations of the crystalline structure and properties allow them to be used for modeling the most important phases in steels, in particular austenite of different compositions [12, 13]. In order to study the impact of Si and Al additives on the elastic characteristics, structure, and energy state of nickel-chromium austenite, the authors of work [14] modeled its crystalline structure in accordance with the $Fe_8Cr_4Ni_4$ formula. To simulate an unordered solution, the atoms of dissolved components were symmetrically arranged in the FCC (face-centered cubic) nodes of the supercell: 2×2×1, based on γ-Fe, which contained 16 atoms. According to the calculation results, it was found that the dissolution of Si in the austenite of the specified composition, additionally alloyed with Al, leads to a decrease in the elastic constants and theoretical hardness and an increase in the plasticity and Poisson coefficient. At the same time, the thermodynamic and electrochemical stability (calculated by the number of electrons at the Fermi level) increases significantly. However, the cited work disregarded the issue of modeling the introduction solutions involving elements such as carbon and nitrogen. Determining the effect of dissolved nitrogen on the crystalline structure and elasticity characteristics of manganese-chromium austenite of the $Fe_{18}Cr_6Mn_8$ formulation by modeling with the use of DFT is reported in paper [15]. Austenite with different carbon content was modeled in study [16]; it was represented in the form of 5×5×5 supercells based on an FCC cell. They contained 125 Fe atoms in the nodes of the crystalline lattice and 1, 7 and 9 C atoms located in the octahedral pores. The results of the reported modeling showed a nonlinear growth of elasticity and shear modules while increasing the amount of dissolved C, which clearly manifests itself with an increase in the amount of dissolved carbon over 5 %. The structure was modeled in the form of a γ-Fe-based superlattice, which contained 32 metal atoms in the nodes of the lattice and 1 nitrogen atom in the octahedral pore located in the center of the lattice. According to the calculation results, the parameter of the lattice of the $Fe_{18}Cr_6Mn_8$ solid solution at nitrogen dissolution increases from 3,507 to 3,522 angstrom (Å), and its formation energy increases by 2–2.5 times. At the same time, the values of modules B and G increase while the Poisson coefficient decreases. However, all the structures studied with different mutual arrangements of Fe and Cr atoms, according to the B/G criterion [17], refer to plastic materials: B/G=2.25–3.25 (higher than 1.75). Determination of the yield strength of high-manganese steels alloyed with Al on the basis of a model that included the DFT calculations of the contribution of short-range ordering energy was carried out in [18]. In contrast to works [15, 16], instead of superlattices, the simulation was performed on the basis of calculating the energy of clusters with an FCC lattice and the octahedral pore filled with carbon in the center. The number and configuration of the atom arrangement resulted from searching for crystalline structures with the lowest ordering energy. As a result, six stable structures of the following formulations were identified: Fe_6Al_8C, Fe_5MnAl_8C, $Fe_4Mn_2Al_8C$, Fe_7Al_7C, Mn_6Al_8C, and $Fe_3Mn_3Al_8C$. Extrapolating the data about these structures on the composition of standard austenite steels has made it possible to determine the strength limit with a margin of error of ~10 %. The Ni and Co influence on the electron structure and the elastic characteristics of austenite of the Fe_4C formulation was studied in work [19]. The simulations were carried out using a DFT procedure employing the CASTEP software for structures with an FCC lattice, whose Fe atoms were replaced with Co and Ni atoms in equal proportions in an amount of ~20 at. %. The resulting equilibrium structures were characterized by the presence of a tetragonal FCC lattice with modified parameters (a=3.7367–3.7451 and c=3.7843–3.8061) compared to austenite of the Fe_4C composition (a=3.7478 Å). All model structures met the criteria for mechanical stability and were plastic materials according to the B/G criterion. At the same time, in a general case, there is a simultaneous dissolution of Co and Ni in austenite of the Fe_4C formula. An analysis of values of the calculated elastic constants for structures with a different arrangement of atoms reveals that in a general case the simultaneous dissolution of Ni and Co leads to the higher values of G and a decrease in the B value and plasticity. The comprehensive approach to determining the elastic characteristics of high-manganese austenite was

reported in work [20], whose authors. in parallel with DFT calculations, performed experimental research by a nanoindentation method [21]. The samples for their experimental study were the coatings applied by magnetron spraying and alloys from pure components containing C in the amount of 0.5–3.0 at. %, and Mn, from 28–30 at. %. The comparison of the calculated and experimental values of the parameters of austenite lattices of different compositions shows that the values of the calculated magnitudes (3.51–3.54 Å) are lower compared to the calculated ones (3.59–3.61). However, the tendency to increase the lattice parameter when increasing the contents of Mn and C is reflected in both calculations and experimental results. The experimental values of the Young modulus are described by theoretical calculations with a ~15 % accuracy and are within 185–220 GPa. At the same time, increasing the carbon content within 0–3 at. % does not lead to a noticeable increase in the elasticity module.

Our generalization of the above data from the scientific literature shows that for the alloyed austenite with the total content of alloying elements dissolved by replacing ≤50 at. % and in the amount of $C \leq 3$ at. %, the lattice parameters are within ~3.45–3.6 Å. The calculated values of the *E, B*, and *G* elasticity modules are within 185–346, 150–280, and 70–150 GPa, respectively. The data that most accurately describe the results from experiments were acquired by using the generalized gradient approximation (GGA) into the Perdew-Burke-Ernzerhof (PBE) images using the CASTEP and VASP programming codes. This allows us to argue that it is expedient to simulate alloyed manganese austenite in the form of an FCC superlattice by their central pore filled with a carbon atom.

3. The aim and objectives of the study

The aim of this study was to establish the impact of Si and Cr additives on the crystalline structure and properties of manganese austenite by experimentally determining the structure parameters and by *ab initio* simulation based on DFT methods.

To achieve the set aim, the following tasks have been solved:

– to determine the phase composition of high-manganese steel and to analyze its Mossbauer spectrum;

– to assess the impact of Si and Cr on the elastic constants, mechanical characteristics, and stability of manganese austenite;

– to establish patterns in the electron structure of manganese austenite with the dissolved atoms of Si and Cr and to establish its relation to the physical-mechanical characteristics.

4. Materials and methodology to study the influence of Si and Cr on the characteristics of manganese austenite

We theoretically determined the parameters of the crystalline structure and elastic constants of manganese austenite depending on its composition within the framework of DFT and pseudopotential methods using the basis of flat waves. The calculations were performed using the CASTEP programming code by the generalized gradient approximation (GGA) method in the representation by Perdew-Burke-Ernzerhof (PBE) [22]. The Brillion's zone was split into a grid of 4×4×4 *k*-points according to the Monkhorst-Pack scheme [23]. We described the potentials of ions by using the ultra-low potentials by Vanderbilt [24] for the electron configurations of ions: C–$2s^2 2p^2$, Si–$3s^2 3p^2$, Mn–3d54s2, Fe–3d64s2. The optimization of the geometry (relaxation of the structure) was considered complete at a volumetric tension of <0.05 GPa and the forces acting on an atom of <0,03 eV/Å. The 2×2×2 supercells based on an FCC lattice with 32 iron atoms and alloying elements per one cell were used to simulate the structure of austenite (Fig. 1). A carbon atom was placed in the central octahedral pore.

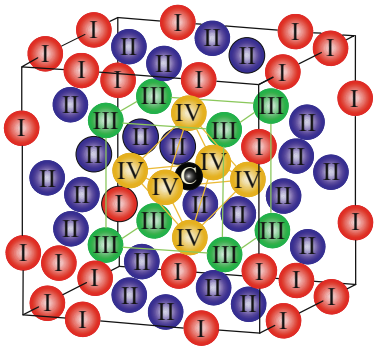

Fig. 1. A model of the crystalline structure of alloyed austenite

In the model superlattice, the following groups of symmetrically arranged atoms can be identified: along the edges (I) and faces (II), as well as at the cube vertices (III), and the octahedron vertices (IV) around the central octahedral pore. Thus, the composition of austenite corresponded to the formula $A_6^I B_{12}^{II} D_8^{III} F_6^{IV} - C$, where A, B, D, F are the alloying elements that form the substitutional solutions with iron in positions I, II, III, IV.

Samples for our experimental study were manufactured by the electric arc fusion of ferrosilicon-manganese and low-carbon steel. Based on the results from an X-ray fluorescence analysis, the composition of the alloys corresponded to high-manganese steel containing, % by weight: Mn ~19 %, Si ~4 %, C ~1.5, the rest – Fe.

We experimentally studied the parameters of the crystalline structure by a Mossbauer spectroscopy method using the nuclear gamma-resonance spectrometer YaGRS-4M. The Fe^{57} electron Mossbauer spectra were acquired by using Co^{57} in the chromium matrix as a source of γ-quants and by calibrating the isometric offsets relative to sodium nitroprusside.

Thermodynamic calculations were carried out using the CALPHAD (CALculation of PHAse Diagrams) procedure employing the OpenCalphad programming code [25] and the thermodynamic functions given in works [26–28].

The phase composition of the samples was determined by X-ray phase analysis (XRD) using the DRON-3M diffractometer in the filtered CuK_α radiation with the subsequent diffractogram processing based on the Rietveld method.

5. The results of studying the crystalline structure and certain mechanical characteristics of the manganese austenite alloyed with Si and Cr

5. 1. The results from the X-ray phase analysis, microstructure study, and Mossbauer spectroscopy of high-manganese steel

The results from the X-ray phase analysis of experimental alloys (Fig. 2, *a*) showed that their base phase is Fe with a face-centered lattice (spatial group Fm-3m). The Fe lattice

parameter was a=3.576 Å, which is close to the parameters of the austenite lattice in Hadfield's steel after casting [29] and in welded joints of 3.60–3.62 Å [30]. The results of studying the microstructure of the experimental alloys obtained during the alloying with Si (Fig. 2, *b*) and Cr (Fig. 2, *c*) show that in both cases the structure of the alloys consists of uneven grains of austenite and eutectics with different morphology. In this case, alloying with Cr leads to the formation of a rougher structure of the austenite-carbide eutectics compared to alloying with Si. This is probably due to the different nature of the carbide phases that make up the eutectics. For alloys, alloyed with Cr, it is thermodynamically beneficial to form carbides of the type $(Fe, Mn, Cr)_7C_3$, while when alloying with Si, there is only the formation of cementite-type carbides $(Fe, Mn)_3C$.

The experimental Mossbauer spectrum of Si, Cr-alloyed manganese austenite is formed by a combination of double and singlet components (Fig. 3). No manifestations of the Seeman nuclear effect are observed, indicating that there are no ^{57}Fe nuclei in a magnetically-ordered state. It could be argued that the α-Fe phase is absent and all Fe atoms are part of the austenite structure. Using the UNIVEM-MS software, subject to the Lorentz form of resonance lines, the experimental spectrum was represented as a superposition of two double and one singlet component. They correspond to the resonant absorption of ^{57}Fe by the nuclei, which are in the crystalline- non-equivalent positions of the lattice. The estimation values of the characteristic parameters of the spectrum components (isomeric shift, quadrupole cleavage) of Lorentzian line shape agree well with the data reported in work [31] when analyzing the spectra of austenite (Table 1). The use of Mossbauer spectroscopy has made it possible to calculate the relative proportion of Fe atoms with different types of close neighbors, which would affect the size of the electric field gradient on the core and determine the quadrupole splitting of a particular component. Comparing the findings, it can be argued that the formation of the observed spectrum layout is a consequence of the presence of carbon and alloying atoms in the near coordinating areas of ^{57}Fe. In this case, doublet 1 corresponds to the crystallographic position of ^{57}Fe number I, doublet 2 – positions number II and IV, singlet 1 – position number III (Fig. 1). Taking into consideration the value of the relative proportion p of Fe atoms in a particular environment (Table 1), the most likely is the localization of Si, Mn, and Cr alloying elements in the austenite superlattice in positions number II, III, and IV.

Based on this conclusion, in the further calculations of the model crystalline structure, the Mn atoms were arranged in the crystallographic position of position III, and the Si or Cr atoms – in position IV. The initial parameter of the superlattice was set to 2×a, where a is the parameter of the austenite lattice, defined experimentally (3.576 Å). This arrangement of atoms ensured that all the necessary pairs of adjacent atoms were available: C-Mn, C-(Si,Cr), C-Fe, Mn-(Si,Cr), Mn-Fe, Fe-(Si,Cr).

Table 1

Results of processing the experimental spectrum of manganese austenite: Q_s – quadrupole uncoupling, mm/s; G – line width, mm/s; p – relative share of Fe atoms, %

Phase	Doublet 1			Doublet 2			Singlet 1	
	Q_s, mm/s	G, mm/s	P	Q_s, mm/s	G, mm/s	P	Q_s, mm/s	P
γ-Fe(Mn,C)	0.65	0.31	38.7	0.16	0.21	50.0	0.18	11.3
γ-$Fe_{10}C$ [31]	0.65	0.30	57.0	0.10	0.24	34.0	0.23	9.0

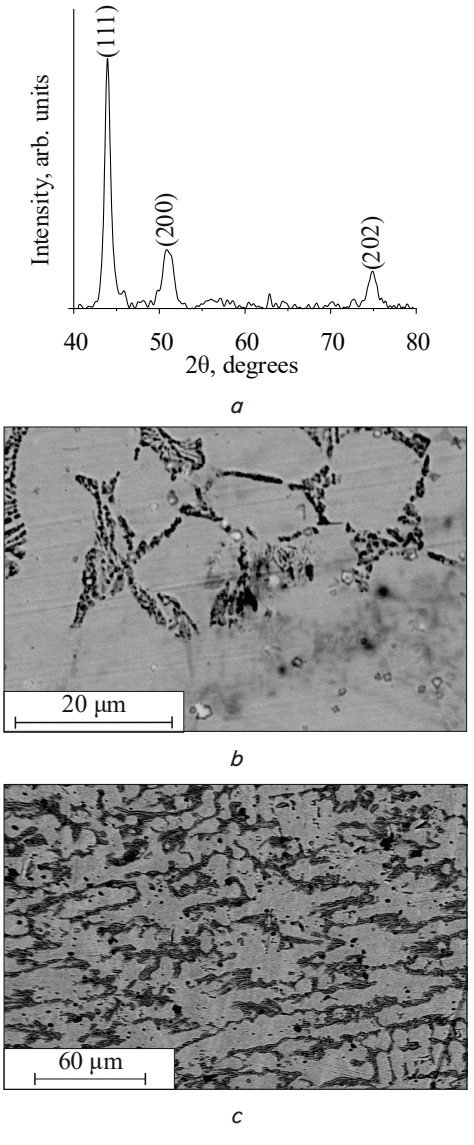

Fig. 2. The analysis of phase composition and microstructure of experimental materials: *a* – diffractogram of high manganese experimental steel; *b* – microstructure of high-manganese steel alloyed with silicon; *c* – microstructure of high-manganese steel alloyed with chrome

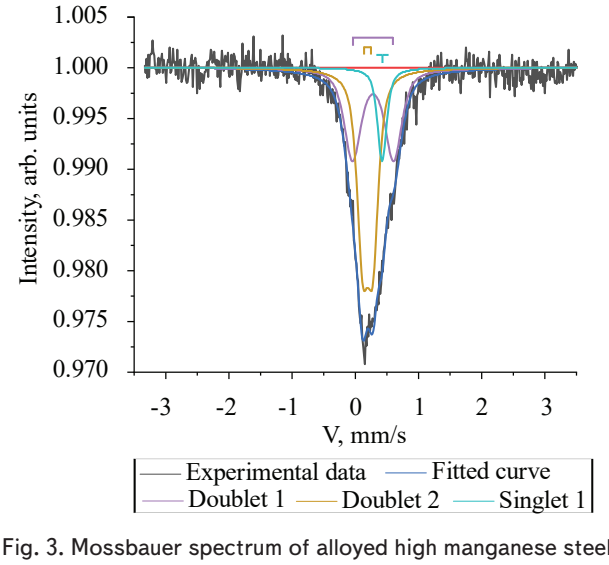

Fig. 3. Mossbauer spectrum of alloyed high manganese steel

The comparative analysis of the parameters of the Mossbauer spectra of carbon and manganese austenite reveals the proximity of the parameters of quadrupole uncoupling and line width, which indicates the stability of the austenite phase in experimental alloys.

5. 2. The results of determining the stability and mechanical characteristics of manganese austenite when dissolving Si and Cr

One of the attributes of stability of a crystalline structure is, in particular, its mechanical stability, which, depending on the type of crystal lattice, is determined by the Bourne-Huang criterion. For a tetragonal lattice, which was the basis for model structures, the stability, depending on the elastic constants (C_{ij}), is determined by meeting a series of criteria: $C_{11}>0$, $C_{33}>0$, $C_{44}>0$, $C_{66}>0$, $C_{11}C_{12}>0$, $C_{11}+C_{33}2C_{12}>0$ and $2(C_{11}+C_{12})+C_{33}+4C_{13}>0$. The elastic constants were calculated after optimizing the geometry (structure relaxation) in accordance with the relationship between deformation and stresses under the generalized Hook law:

$$\sigma_{ij}=C_{ij}\varepsilon_{kl}, \quad (1)$$

where σ_{ij} is the stretching strain; ε_{kl} is the longitudinal deformation.

Comparing the results of our calculations of values for the elastic constants, the lattice parameter (a), and the full energy of the crystalline lattice (Et) for pure γ-Fe, according to the selected methodology, to the data reported in [32] shows that they are in good agreement (Table 2).

Table 2

Characteristics of the crystalline structure of γ-Fe

Elastic constants	C_{11}	C_{12}	C_{44}	a, Å	Et, eV/atom
Calculation	445.591	204.884	254.627	3.45342	–27,685.6
Data from [32]	484	234	287	3.45	–34,634.5

The elastic constants and the parameters of the model structures' lattices are given in Table 3. An analysis of them shows that the value of the austenite (Fe-C) lattice parameter (3.5743 Å), calculated by extrapolating the empirical equation proposed in work [33] to T=0 K, and that of the model structure are within the typical error for calculations based on a DFT method (10 %).

The resulting values of the elastic constants are the initial ones to calculate some mechanical characteristics of a polycrystalline material [34]. According to the average Voight-Reuss-Hill (VRH) scheme [35], the values of the volumetric elasticity module (B) and the shear module (G) are determined from the following equations:

$$B=\frac{1}{9}(C_{11}+C_{22}+C_{33})+\frac{2}{9}(C_{12}+C_{13}+C_{23}), \quad (2)$$

$$G=\frac{1}{15}(C_{11}+C_{22}+C_{33}-C_{12}-C_{13}-C_{23})+$$
$$+\frac{1}{5}(C_{44}+C_{55}+C_{66}). \quad (3)$$

Given the known values of B and G for polycrystalline structures, the Young module (E) and the Poisson coefficient (v) can be calculated from the following equations:

$$E=\frac{9GB}{G+3B}, \quad (4)$$

$$v=\frac{3B-2G}{2(G+3B)}. \quad (5)$$

We assessed hardness (theoretical) according to Vickers by using a Lyakhov-Oganov procedure, whereby the Knoop hardness is calculated from the equation given in [36]:

$$HK=\frac{423.8}{V}n\left(\prod_{k=1}^{n}N_kX_ke^{-2.7f_k}\right)^{1/n}-3.4, \quad (5)$$

where V is the volume of the crystalline lattice, N_k is the number of k-type bonds in the crystalline lattice. X_k and f_k are the energy of holding electrons of the type k bonds and the indicator of ionization, which are determined from the following equations:

$$X_k=\sqrt{\frac{X_i^kX_j^k}{CN_i^kCN_j^k}}$$

and

$$f_k=\frac{X_i^k-X_j^k}{4\sqrt{X_i^kX_j^k}},$$

where X_i^k, X_j^k are the electronegativity of atoms i, j; and CN_j^k is their coordination number.

The anisotropy (A_z) of a crystalline structure with cubic symmetry at known values of the elastic constants is determined from a Zener ratio:

$$A_z=\frac{2C_{44}}{(C_{11}-C_{12})}. \quad (6)$$

For completely isotropic crystalline structures, A_z=1.

Table 3

Calculated values of elastic constants and parameters of the model structures' lattices

Elastic constants	C_{11}	C_{12}	C_{13}	C_{33}	C_{44}	C_{66}	a, Å
$Fe_{32}C$	451.21	199.848	199.848	451.21	221.318	221.318	3.4754
$Fe_{24}Mn_8C$	421.46	215.519	215.519	421.46	221.934	221.934	3.4863
$Fe_{18}Mn_8Si_6C$	325.404	191.274	191.274	325.404	97.588	97.588	3.5294
$Fe_{18}Mn_8Cr_6C$	282.433	152.656	152.656	282.433	144.541	144.541	3.5162

The results of our calculations (Fig. 4) show that the dissolution of C and the studied alloying elements (Mn, Si, Cr), forming substitutional solutions, leads to the growth of the γ-Fe lattice parameter. This is accompanied by the growth of thermodynamic stability of the austenite phase. Dissolving Mn in austenite leads to a slight decrease in the values of modules E and G and the growth of module B. In this case, there is an increase in plasticity, hardness, thermodynamic stability. Dissolution of Si and Cr in manganese austenite leads to its increased thermodynamic stability, hardness, and plasticity, while the values of elasticity modules (B, G, and E) decrease.

The effect of silicon on the change in these characteristics manifests itself more clearly. However, dissolution of silicon leads to a decrease in the anisotropy of the austenite phase (A_z) while, when dissolving Cr, anisotropy increases.

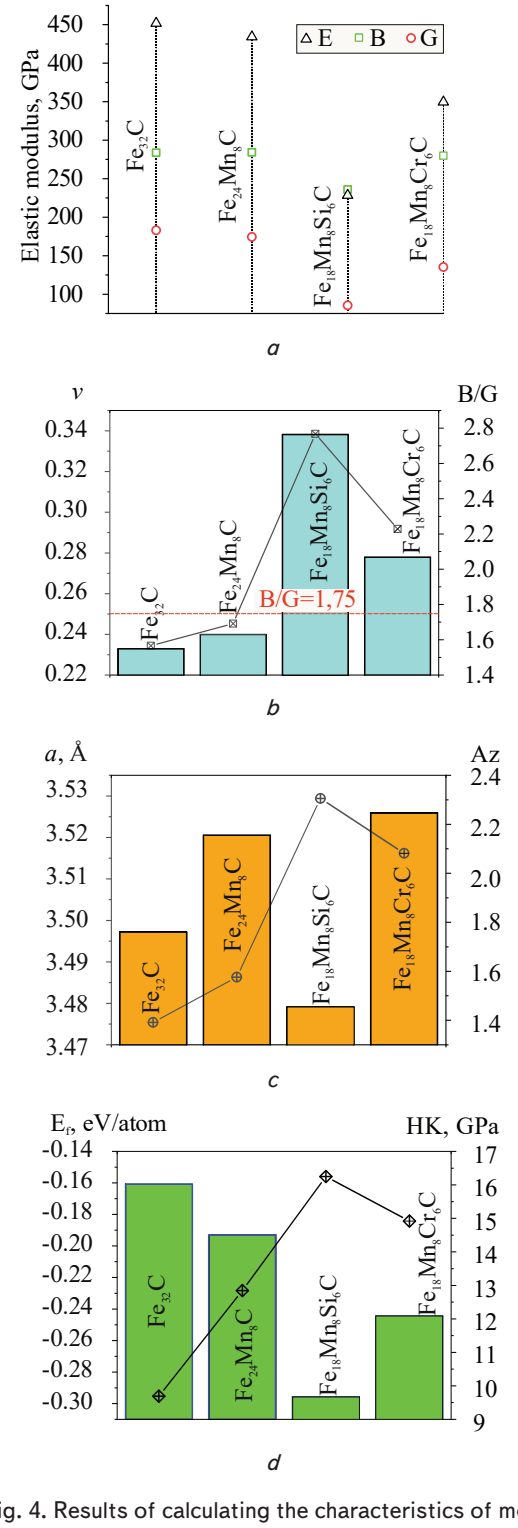

Fig. 4. Results of calculating the characteristics of model austenite structures: *a* – elastic constants; *b* – plasticity and Poisson coefficient; *c* – the parameter of lattice and anisotropy; *d* – stability and theoretical hardness

The analysis of Gibbs energy temperature dependences (G_m) of alloys, whose composition corresponds to the model structures (Fig. 5), calculated according to the CALPHAD methodology, shows the same tendencies to stabilize the austenite phase as the DFT calculations. In particular, the dissolution of *C* leads to a slight decrease in G_m in the temperature stability region γ-Fe (~1,184–1,665 K), according to the equilibrium Fe state diagram. Further dissolution of Mn leads to a significant decrease in the G_m of the austenite phase, which is observed throughout the entire temperature range (800–1,800 K). With the simultaneous dissolution of Mn and Si, the intensity of reducing the free energy of austenite increases by almost two times, compared to Fe-C alloys, where only Mn dissolved. Dissolution of Cr in manganese austenite also leads to a decrease in its Gibbs energy but, compared to Si, its effect is much weaker.

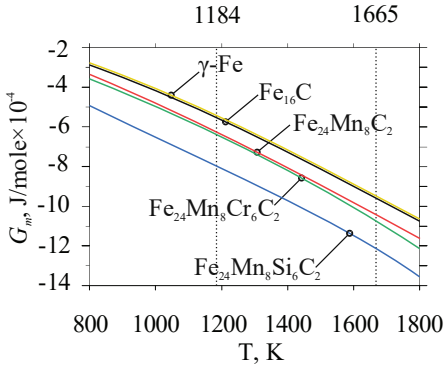

Fig. 5. Gibbs energy temperature dependence of alloys corresponding to model structures: γ-Fe, $Fe_{16}C$, $Fe_{27}Mn_5C_2$, and $Fe_{24}Mn_5Si_3C_2$

The DFT calculation data at 0 K agree well with the CALPHAD thermodynamic calculations at 800–1,600 K. This indicates that the identified trends in the impact of Si and Cr on elastic constants would be maintained under normal conditions and elevated temperatures.

5. 3. The results of analyzing the electron structure of manganese austenite when dissolving Si and Cr

The calculated density of electron states (DOS) of austenite structures (Fig. 6) indicates the similarity of their electron structure, and the lack of energy cracks near the Fermi level (zero energy point) is a sign of the bond of metallic type. According to [14], the number of electrons at the Fermi level determines the level of electrochemical stability of a structure, namely, when it increases, the level of stability decreases. According to this, the model austenite structures in the order of growth of their electrochemical stability can be placed in a series: $Fe_{32}C \rightarrow Fe_{24}Mn_8C(Fe_{18}Mn_8Si_6C) \rightarrow Fe_{18}Mn_8Cr_6C$. Thus, dissolving Mn in austenite increases its electrochemical stability while the further dissolution of Si in it does not significantly affect its value. In this case, the dissolution of Cr in manganese austenite leads to a significant increase in electrochemical stability, which can manifest in the growth of corrosion resistance.

The analysis of electron distribution density maps for model structures in the plane (002) (Fig. 7) shows that interatomic bonds with high concentrations of Fe-C and Cr-C electrons are formed in $Fe_{24}Mn_8C$ and $Fe_{18}Mn_8Si_6C$ structures, respectively. For the $Fe_{18}Mn_8Si_6C$ structure, the density of electrons in Si–C pairs is much lower but the relatively high density of electrons is found in Fe-Si pairs. Bonds

in pairs of metal-carbon are characterized by a covalent type, which, in a general case, is reflected on the mechanical properties such as a decrease in plasticity. Therefore, the nature of the distribution of electron density indicates that, for $Fe_{24}Mn_8C$, the plasticity would be lower compared to $Fe_{18}Mn_8Si_6C$. For $Fe_{18}Mn_8Si_6C$, the low concentration of electrons around the C atom implies the increased plasticity, on the one hand, while the presence of the developed covalent metal bonds metal–silicon increases hardness, on the other hand.

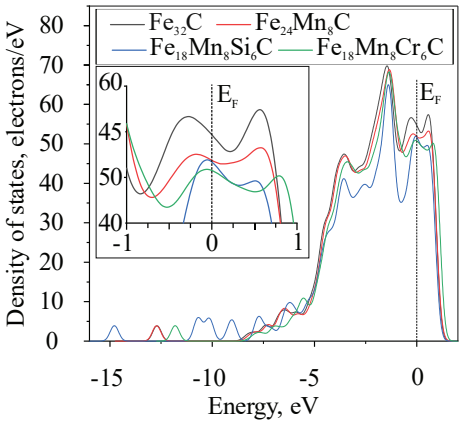

Fig. 6. Complete density of electron states of austenite of different formulation

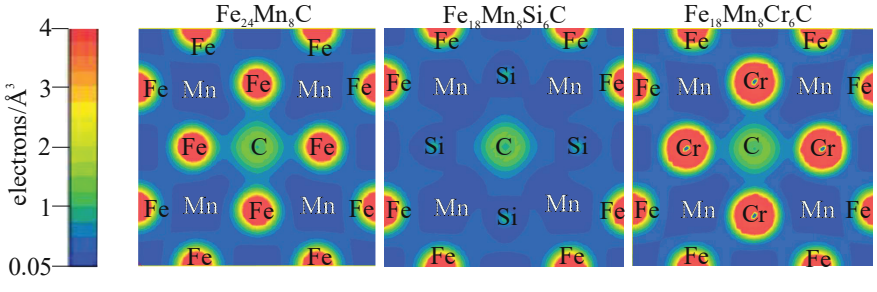

Fig. 7. Maps of the electron density distribution of model structures in the plane (200)

Thus, the dissolution of Si and Cr in both cases causes significant enough changes in the distribution of the density of electrons, which leads to a simultaneous increase in the hardness and plasticity indicators of the austenite phase.

6. Discussion of results of analyzing the impact of alloying with Si and Cr on the structure of manganese austenite

The generalization of results from our experimental research and the results of modeling shows that the dissolution of Si and Cr leads to the increased stability of the austenite phase (Fig. 4, *d*). Increasing the stability of austenite (Fig. 5) is a prerequisite for preventing the process of cement phase evolution, which negatively affects the capability of manganese austenite to be used for surfacing. On the other hand, the dissolution of Si and Cr leads to changes in mechanical characteristics, in particular to a decrease in the elastic constants (Fig. 4, *a*) and an increase in plasticity (Fig. 4, *b*). The theoretical hardness of manganese austenite, calculated from equation (5) (Fig. 4, *d*), correlates with the level of its stability and the nature of the formation of interatomic bonds (Fig. 5, 7). When dissolving Si in manganese austenite, its stability is higher than when dissolving Cr; hence, its theoretical hardness is also higher although the level of electrochemical stability (Fig. 6) is higher when dissolving Cr.

Our results are useful for the development of new systems to alloy materials for wear-resistant surfacing based on high-manganese steel, under operating conditions involving dynamic and cyclical loads. The scope of application of such materials includes the working surfaces of milling units, agricultural machinery, as well as equipment for woodworking and processing of timber biomass.

The main limitation in the use of our data in relation to actual systems is the need to extrapolate them to the ratio of components that cannot be set for supercells (Fig. 1) due to a significant labor intensity of calculations. In addition, due to the presence of defects in actual structures, such as vacancies, dislocations, grain boundaries, etc., the calculated hardness values could mainly be used for a comparative analysis only.

The presence of Si dissolved in the austenite is a prerequisite for the fundamental possibility of applying coatings by electric arc methods, that is, Si is primarily a technological additive. In contrast to Si, introducing Cr into austenite aims to enhance performance, namely corrosion resistance and hardness. Based on this, further studies should investigate the total impact of Si and Cr, as well as other carbide-forming elements that may dissolve in small quantities in manganese austenite.

7. Conclusions

1. It was established that the main phase in high-manganese steel, containing, % by weight: Mn ~19 %, Si ~4 %, C ~1.5, made by electric arc fusion, is γ-Fe with a lattice parameter of a=3.576 Å. Analyzing it by a Mossbauer spectroscopy method shows that the Si and Mn dissolved in γ-Fe mainly occupy those positions in the lattice relative to which the carbon atom is in the first or second coordinating sphere.

2. The *ab initio* simulation and the thermodynamic calculations using a CALPHAD method helped establish that dissolving Si and Cr in manganese austenite leads to an increase in its stability. In this case, plasticity and theoretical hardness increase while the value of elastic constants decreases. Si dissolution has a more significant impact compared to Cr, both to increase the stability of austenite and to change its mechanical characteristics.

3. Based on the results of calculating the density of electron states, it is found that the dissolution of Si and Cr does not significantly affect the electron structure of manganese austenite. This, in particular, indicates that the stacking fault energy (SFE) value would not change significantly, and, consequently, the mechanism of the deformation strengthening of manganese austenite would not change. The lowest density of electron states at the Fermi level was found for the manganese austenite alloyed with chromium, indicating the highest level of its electrochemical stability among the structures examined.

References

1. Vitos, L., Nilsson, J.-O., Johansson, B. (2006). Alloying effects on the stacking fault energy in austenitic stainless steels from first-principles theory. Acta Materialia, 54 (14), 3821–3826. doi: http://doi.org/10.1016/j.actamat.2006.04.013
2. Ostapovets, A. (2010). Atomistic model of type-II twin boundary. Computational Materials Science, 49 (4), 882–887. doi: http://doi.org/10.1016/j.commatsci.2010.06.041
3. Mosecker, L., Saeed-Akbari, A. (2013). Nitrogen in chromium–manganese stainless steels: a review on the evaluation of stacking fault energy by computational thermodynamics. Science and Technology of Advanced Materials, 14 (3), 033001. doi: http://doi.org/10.1088/1468-6996/14/3/033001
4. Tatsiy, R. M., Pazen, O. Y., Vovk, S. Y., Ropyak, L. Y., Pryhorovska, T. O. (2019). Numerical study on heat transfer in multilayered structures of main geometric forms made of different materials. Journal of the Serbian Society for Computational Mechanics, 13 (2), 36–55. doi: http://doi.org/10.24874/jsscm.2019.13.02.04
5. Volchenko, N., Volchenko, A., Volchenko, D., Poliakov, P., Malyk, V., Zhuravliov, D. et. al. (2019). Features of the estimation of the intensity of heat exchange in self-ventilated disk-shoe brakes of vehicles. Eastern-European Journal of Enterprise Technologies, 1 (5 (97)), 47–53. doi: http://doi.org/10.15587/1729-4061.2019.154712
6. Ropyak, L., Ostapovych, V. (2016). Optimization of process parameters of chrome plating for providing quality indicators of reciprocating pumps parts. Eastern-European Journal of Enterprise Technologies, 2 (5 (80)), 50–62. doi: http://doi.org/10.15587/1729-4061.2016.65719
7. Drábiková, J., Pastorek, F., Fintová, S., Doležal, P., Wasserbauer, J. (2016). Improvement of bio-compatible AZ61 magnesium alloy corrosion resistance by fluoride conversion coating. Koroze a Ochrana Materialu, 60 (5), 132–138. doi: http://doi.org/10.1515/kom-2016-0021
8. Saakiyan, L. S., Efremov, A. P., Ropyak, L. Ya. (1989). Effect of stress on the microelectrochemical heterogeneity of steel. Protection of Metals, 25 (2), 185–189.
9. Kresse, G., Furthmüller, J. (1996). Efficiency of ab-initio total energy calculations for metals and semiconductors using a plane-wave basis set. Computational Materials Science, 6 (1), 15–50. doi: http://doi.org/10.1016/0927-0256(96)00008-0
10. Hafner, J., Kresse, G. (1997). The Vienna AB-Initio Simulation Program VASP: An Efficient and Versatile Tool for Studying the Structural, Dynamic, and Electronic Properties of Materials. Properties of Complex Inorganic Solids, 69–82. doi: http://doi.org/10.1007/978-1-4615-5943-6_10
11. Clark, S. J., Segall, M. D., Pickard, C. J., Hasnip, P. J., Probert, M. I. J., Refson, K., Payne, M. C. (2005). First principles methods using CASTEP. Zeitschrift Für Kristallographie – Crystalline Materials, 220 (5/6). 567–570. doi: http://doi.org/10.1524/zkri.220.5.567.65075
12. Duryagina, Z. A., Bespalov, S. A., Borysyuk, A. K., Pidkova, V. Ya. (2011). Magnetometric analysis of surface layers of 12X18H10T steel after ion-beam nitriding. Metallofizika i noveishie tekhnologii, 33 (5), 615–622.
13. Tatarenko, V. A., Radchenko, T. M., Nadutov, V. M. (2003). Parameters of interatomic interaction in a substitutional alloy F.C.C. Ni-Fe according to experimental data about the magnetic characteristics and equilibrium values of intensity of a diffuse scattering of radiations. Metallofizika i noveishie tekhnologii, 25 (10), 1303–1319.
14. Dong, N., Jia, R., Wang, J., Fan, G., Fang, X., Han, P. (2019). Composition Optimum Design and Strengthening and Toughening Mechanisms of New Alumina-Forming Austenitic Heat-Resistant Steels. Metals, 9 (9), 921. doi: http://doi.org/10.3390/met9090921
15. Zhou, Y., Li, Y., Wang, W., Qian, L., Xiao, S., Lv, Z. (2018). Effect of interstitial nitrogen in $Fe_{18}Cr_6Mn_8$ austenitic alloys from density functional theory. Journal of Magnetism and Magnetic Materials, 463, 57–63. doi: http://doi.org/10.1016/j.jmmm.2018.05.034
16. Oila, A., Bull, S. J. (2009). Atomistic simulation of Fe–C austenite. Computational Materials Science, 45 (2), 235–239. doi: http://doi.org/10.1016/j.commatsci.2008.09.013
17. Lv, Z. Q., Wang, B., Sun, S. H., Fu, W. T. (2015). Effect of atomic sites on electronic and mechanical properties of $(Fe,Mo)_6C$ carbides. Journal of Alloys and Compounds, 649, 1089–1093. doi: http://doi.org/10.1016/j.jallcom.2015.06.249
18. Sevsek, S., Bleck, W. (2018). Ab Initio-Based Modelling of the Yield Strength in High-Manganese Steels. Metals, 8 (1), 34. doi: http://doi.org/10.3390/met8010034
19. Lv, Z. Q., Shi, Z. P., Li, Y. (2012). First-Principles Study on the Structural, Electronic and Elastic Properties of Alloyed Austenite with Co and Ni. Advanced Materials Research, 503-504, 684–687. doi: http://doi.org/10.4028/www.scientific.net/amr.503-504.684
20. Reeh, S., Music, D., Gebhardt, T., Kasprzak, M., Jäpel, T., Zaefferer, S. et. al. (2012). Elastic properties of face-centred cubic Fe–Mn–C studied by nanoindentation and ab initio calculations. Acta Materialia, 60 (17), 6025–6032. doi: http://doi.org/10.1016/j.actamat.2012.07.038
21. Guo, T., Siska, F., Cheng, J., Barnett, M. (2018). Initiation of basal slip and tensile twinning in magnesium alloys during nanoindentation. Journal of Alloys and Compounds, 731, 620–630. doi: http://doi.org/10.1016/j.jallcom.2017.10.088
22. Perdew, J. P., Burke, K., Ernzerhof, M. (1997). Generalized Gradient Approximation Made Simple. Physical Review Letters, 78 (7), 1396–1405. doi: http://doi.org/10.1103/physrevlett.78.1396
23. Monkhorst, H. J., Pack, J. D. (1976). Special points for Brillouin-zone integrations. Physical Review B, 13 (12), 5188–5192. doi: http://doi.org/10.1103/physrevb.13.5188

24. Vanderbilt, D. (1990). Soft self-consistent pseudopotentials in a generalized eigenvalue formalism. Physical Review B, 41 (11), 7892–7895. doi: http://doi.org/10.1103/physrevb.41.7892
25. Sundman, B., Kattner, U. R., Palumbo, M., Fries, S. G. (2015). OpenCalphad - a free thermodynamic software. Integrating Materials and Manufacturing Innovation, 4 (1), 1–15. doi: http://doi.org/10.1186/s40192-014-0029-1
26. Hallstedt, B., Khvan, A. V., Lindahl, B. B., Selleby, M., Liu, S. (2017). PrecHiMn-4 – A thermodynamic database for high-Mn steels. Calphad, 56, 49–57. doi: http://doi.org/10.1016/j.calphad.2016.11.006
27. Shihab, T., Prysyazhnyuk, P., Semyanyk, I., Anrusyshyn, R., Ivanov, O., Troshchuk, L. (2020). Thermodynamic Approach to the Development and Selection of Hardfacing Materials in Energy Industry. Management Systems in Production Engineering, 28 (2), 84–89. doi: http://doi.org/10.2478/mspe-2020-0013
28. Prysyazhnyuk, P., Lutsak, D., Vasylyk, A., Shihab, T., Burda, M. (2015). Calculation of surface tension and its temperature dependence for liquid Cu-20Ni-20Mn alloy. Management Systems in Production Engineering, 12, 346–350.
29. Kryl', Y. A., Prysyazhnyuk, P. M. (2013). Structure formation and properties of NbC-Hadfield steel cermets. Journal of Superhard Materials, 35 (5), 292–297. doi: http://doi.org/10.3103/s1063457613050043
30. Sabzi, M., Dezfuli, S. M. (2018). Post weld heat treatment of hypereutectoid hadfield steel: Characterization and control of microstructure, phase equilibrium, mechanical properties and fracture mode of welding joint. Journal of Manufacturing Processes, 34, 313–328. doi: http://doi.org/10.1016/j.jmapro.2018.06.009
31. Timoshevskii, A. M., Yablonovskii, S. O., Yeremin, V. I. (2011). Computer Simulation of Atomic Structure and Hyperfine Interactions in Fe–C Austenite. Uspehi Fiziki Metallov, 12 (4), 451–470. doi: http://doi.org/10.15407/ufm.12.04.451
32. Guo, G. Y., Yablonovskii, S. O., Wang, H. H. (2000). Gradient-corrected density functional calculation of elastic constants of Fe, Co and Ni in bcc, fcc and hcp structures. Chinese Journal of Physics, 38 (5), 949–961.
33. Seki, I., Nagata, K. (2005). Lattice Constant of Iron and Austenite Including Its Supersaturation Phase of Carbon. ISIJ International, 45 (12), 1789–1794. doi: http://doi.org/10.2355/isijinternational.45.1789
34. Sahalianov, I. Y., Radchenko, T. M., Tatarenko, V. A., Cuniberti, G., Prylutskyy, Y. I. (2019). Straintronics in graphene: Extra large electronic band gap induced by tensile and shear strains. Journal of Applied Physics, 126 (5), 054302. doi: http://doi.org/10.1063/1.5095600
35. Wu, Z., Zhao, E., Xiang, H., Hao, X., Liu, X., Meng, J. (2007). Crystal structures and elastic properties of superhard IrN_2 and IrN_3 from first principles. Physical Review B, 76 (5). doi: http://doi.org/10.1103/physrevb.76.054115
36. Lyakhov, A. O., Oganov, A. R. (2011). Evolutionary search for superhard materials: Methodology and applications to forms of carbon and TiO_2. Physical Review B, 84 (9). doi: http://doi.org/10.1103/physrevb.84.092103